In Vivo High-Resolution Conductivity Imaging of the Human Leg Using MREIT: The First Human Experiment

Hyung Joong Kim, Young Tae Kim, Atul S. Minhas, Woo Chul Jeong, Eung Je Woo*, *Member, IEEE*, Jin Keun Seo, and O Jung Kwon

***Abstract*—We present the first *in vivo* cross-sectional conductivity image of the human leg with 1.7 mm pixel size using the magnetic resonance electrical impedance tomography (MREIT) technique. After a review of its experimental protocol by an Institutional Review Board (IRB), we performed MREIT imaging experiments of four human subjects using a 3 T MRI scanner. Adopting thin and flexible carbon–hydrogel electrodes with a large surface area and good contact, we could inject as much as 9 mA current in a form of 15 ms pulse into the leg without producing a painful sensation and motion artifact. Sequentially injecting two imaging currents in two different directions, we collected induced magnetic flux density data inside the leg. Scaled conductivity images reconstructed by using the single-step harmonic B_z algorithm well distinguished different parts of the subcutaneous adipose tissue, muscle, crural fascia, intermuscular septum and bone inside the leg. We could observe spurious noise spikes in the outer layer of the bone primarily due to the MR signal void phenomenon there. Around the fat, the chemical shift of about two pixels occurred obscuring the boundary of the fat region. Future work should include a fat correction method incorporated in the MREIT pulse sequence and improvements in radio-frequency coils and image reconstruction algorithms. Further human imaging experiments are planned and being conducted to produce conductivity images from different parts of the human body.**

***Index Terms*—Conductivity image, *in vivo* human imaging, magnetic resonance electrical impedance tomography (MREIT).**

I. Introduction

When we inject current into the human body using a pair of surface electrodes, it forms an internal current density distribution, which is determined by the conductivity distribution inside the body [1], [2]. The current density induces a magnetic flux density distribution $\mathbf{B} = (B_x, B_y, B_z)$ and we can measure it using an magnetic resonance imaging (MRI) scanner. Without rotating the human body inside the MRI scanner, only B_z data is measurable when z is the direction of the main magnetic field of the MRI scanner [3].

Cross-sectional imaging of the conductivity distribution has been suggested in magnetic resonance electrical impedance tomography (MREIT) where measured B_z data sets subject to multiple injection currents are utilized [4]–[10]. Previous imaging experiments in MREIT using conductivity phantoms have shown that spatial resolution of a conductivity image is comparable to that of a conventional MR image if enough currents are injected [11]–[13]. Recent postmortem and *in vivo* animal imaging studies demonstrated that we can produce high-resolution conductivity images of intact animals [14]–[17].

Following the latest animal imaging experiment, we have tried the first human imaging experiment in MREIT. As the imaging area, we chose the lower extremity including the subcutaneous adipose tissue, muscle and bone. This paper describes the experimental procedure using carbon–hydrogel electrodes. Presenting results of the experiment, we discuss future research directions toward clinical applications.

II. Methods

A. Carbon–Hydrogel Electrode and MREIT Current Source

Fig. 1(a) shows the carbon–hydrogel electrode we adopted for human imaging experiments. It comprises a custom-designed carbon electrode and a layer of hydrogel with adhesive (HUREV Co. Ltd., Korea). The sizes of the carbon electrode and hydrogel layer are $80 \times 60 \times 0.06$ mm^3 and $80 \times 60 \times 5.7$ mm^3, respectively. The conductivity values of the carbon and hydrogel are 2.857×10^4 and 0.17 S/m, respectively.

Since it is thin and flexible, the experimental procedure to attach the electrode is significantly simplified compared with the previously used rigid recessed electrodes [15], [16]. The 5.7-mm hydrogel layer recessed the thin carbon electrode from the skin and this design was enough to prevent radio-frequency (RF) shielding artifacts from occurring inside the imaging object. Since the new electrode with adhesive does not require an electrode holder, geometrical distortion of the imaging object was minimized. The performance of the new electrode was validated through repeated MREIT scans of conductivity phantoms and postmortem swine legs [17], [18].

To inject imaging currents into a human subject, we used a custom-designed MREIT current source with an isolated linear power supply [19]. We measured a leakage current using an

Manuscript received January 23, 2009; revised March 04, 2009. First published April 14, 2009; current version published October 28, 2009. This work was supported by the Korea Science and Engineering Foundation (KOSEF) grant funded by the Korea government (MEST) (R11-2002-103). *Asterisk indicates corresponding author.*

H. J. Kim, Y. T. Kim, A. S. Minhas, and W. C. Jeong are with the Department of Biomedical Engineering, Kyung Hee University, Yongin, Gyeonggi, 446-701 Korea.

*E. J. Woo is with the Department of Biomedical Engineering, Kyung Hee University, Yongin, Gyeonggi, 446-701 Korea (e-mail: ejwoo@khu.ac.kr).

J. K. Seo is with the Department of Mathematics, Yonsei University, Seoul 120-749, Korea.

O. J. Kwon is with the Division of Pulmonary and Critical Care Medicine, Department of Medicine, Samsung Medical Center, Sungkyunkwan University School of Medicine, Seoul 135-710, Korea.

Color versions of one or more of the figures in this paper are available online at http://ieeexplore.ieee.org.

Digital Object Identifier 10.1109/TMI.2009.2018112

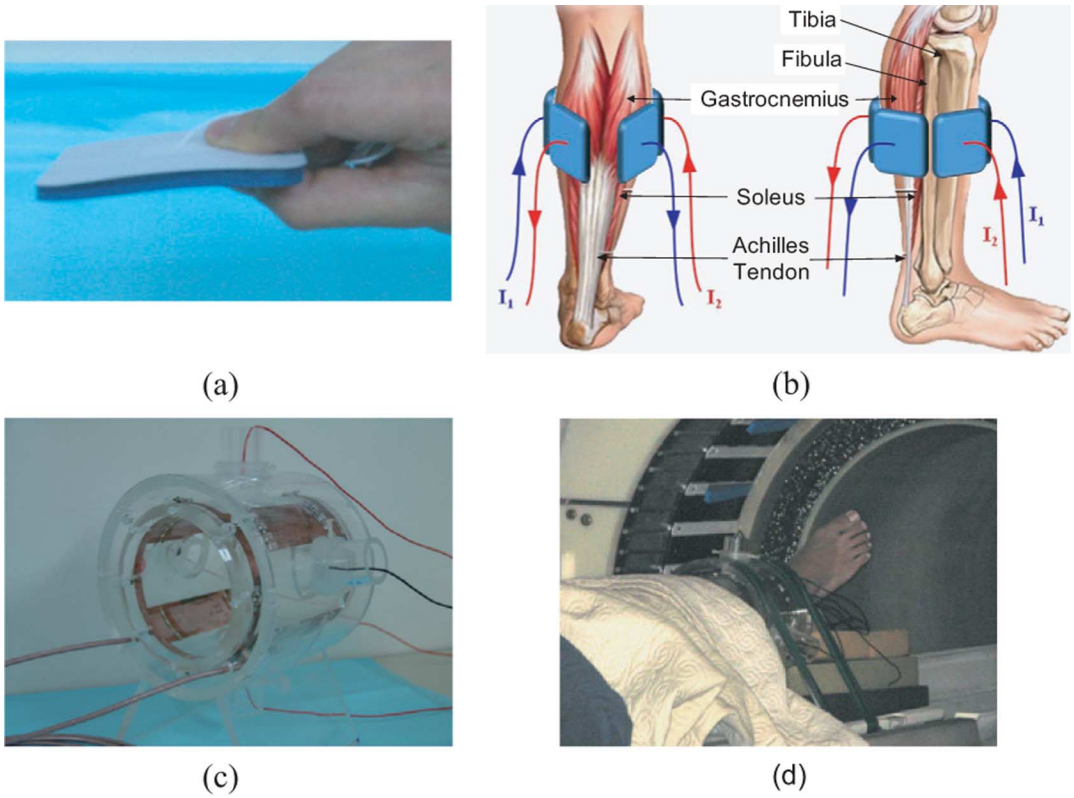

Fig. 1. (a) Carbon–hydrogel electrode. (b) Electrode attachment. (c) RF coil. (d) Imaging setup inside the bore.

TABLE I
CURRENT SOURCE SETUP FOR THE FOUR HUMAN SUBJECTS. HORIZONTAL AND VERTICAL DIRECTIONS ARE DENOTED AS H AND V, RESPECTIVELY, AND THEY MEAN THE CURRENT INJECTIONS USING ONE FACING PAIR OF ELECTRODES AND THE OTHER

Subject	Male A		Male B		Female A		Female B	
Injection Direction	H	V	H	V	H	V	H	V
Sensation Threshold [mA]	1.5	1.0	1.0	1.0	1.5	1.5	2.0	1.5
Pain Threshold [mA]	10.0	9.5	8.0	7.5	9.5	9.5	10.0	10.0
Imaging Current Amplitude [mA]	9.0	9.0	7.0	7.0	9.0	9.0	9.0	9.0

electrical safety analyzer (234A, DNI Nevada). The leakage currents through lead wires and the ground conductor were about 17 μA under the single fault condition.

B. Experimental Procedure

Four healthy volunteers participated in the imaging experiment. We call them male A (26 years old, 60 Kg) and B (29 years old, 58 Kg) and female A (23 years old, 51 Kg) and B (24 years old, 55 Kg) in this paper. The experimental protocol was approved by the Institutional Review Board (IRB) of Samsung Medical Center, Seoul, Korea.

The most critical part was the setup of the current source for current injections. After attaching four electrodes around the leg as shown in Fig. 1(b), we chose one pair of electrodes facing each other to inject current. Starting from 0 mA, we gradually increased the amplitude of the injection current pulse. Subject's oral response was recorded to mark current amplitudes at thresholds of sensation and pain. The same procedure was repeated for the other pair of electrodes. The amplitude of imaging current was determined as less than 95% of the smaller pain threshold. Table I summarizes the current source setup for the four subjects.

With the leg of the human subject positioned inside the RF coil, we placed the subject in the bore of our 3 T MRI scanner (Magnum 3, Medinus, Korea), as shown in Fig. 1(c) and (d). We used the injection current nonlinear encoding (ICNE) pulse sequence [20]. The width of the first current pulse between 90° and 180° RF pulses was 12.5 ms and the second current pulse after 180° RF pulse had the width of 15 ms. Imaging parameters were as follows: $\mathrm{TR/TE} = 1200/30$ ms, $\mathrm{FOV} = 220 \times 220$ mm^2, slice thickness $= 4$ mm, $\mathrm{NEX} = 10$, matrix size $= 128 \times 128$, number of slices $= 8$, and total imaging time $= 100$ min. Fat suppression using a chemical shift selective (CHESS) presaturation pulse [21] was applied to female B only who was the last subject.

C. Conductivity Image Reconstruction

We used the single-step harmonic B_z algorithm for conductivity image reconstructions [11], [22] and produced scaled conductivity images providing contrast information only [23]. Muscles are known to be anisotropic with higher conductivity value in the longitudinal direction compared with the transversal direction [24]–[27]. Since the harmonic B_z algorithm assumes an isotropic conductivity distribution, reconstructed images must be interpreted as equivalent isotropic conductivity images

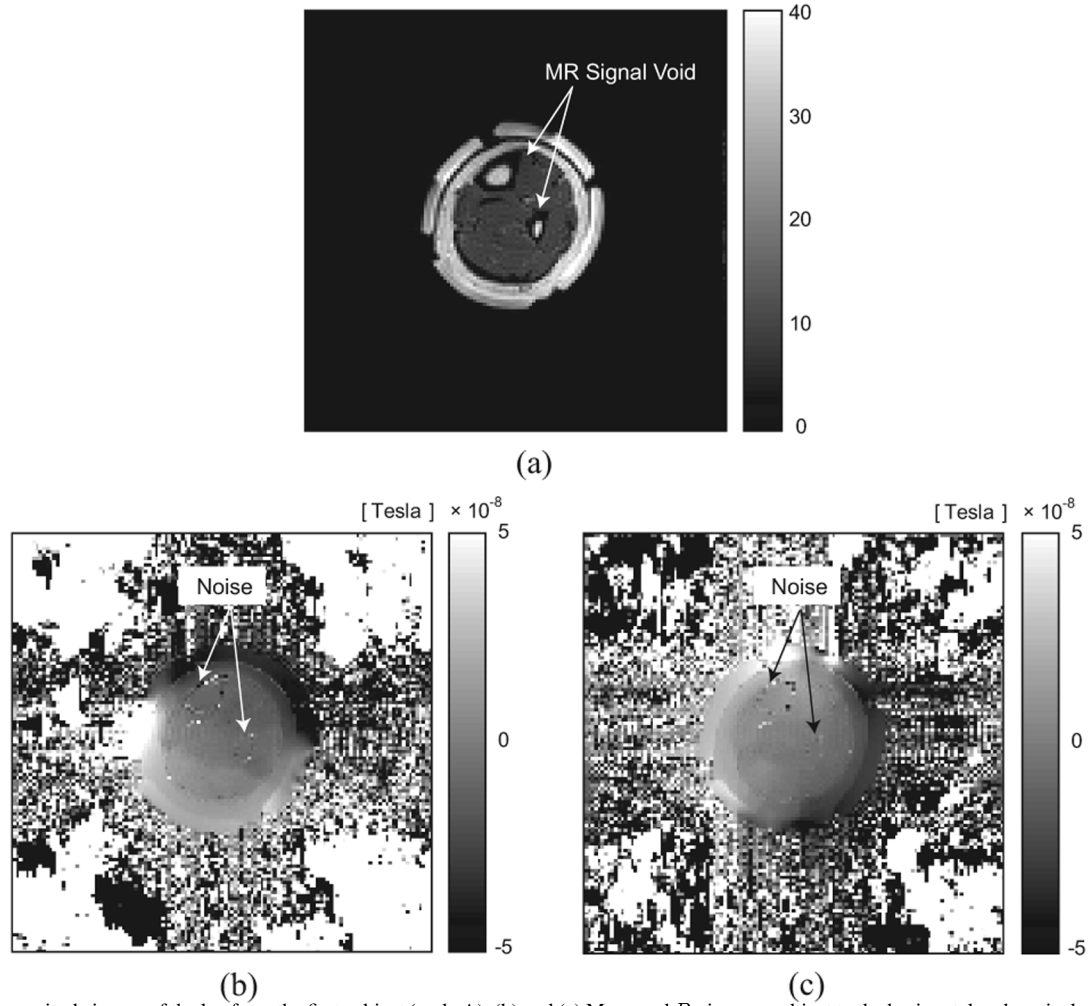

Fig. 2. (a) MR magnitude image of the leg from the first subject (male A). (b) and (c) Measured B_z images subject to the horizontal and vertical current injections, respectively.

[15]. Considering the electrode attachment method shown in Fig. 1(b), a reconstructed conductivity value of the muscle should be understood as a value closer to the conductivity along its transversal direction.

In our previous experimental MREIT studies, we have used an MREIT toolbox for Matlab (Mathworks, Natick, MA) [28]. Lately, Jeon *et al.* developed an MREIT software package with an efficient graphical user interface [29]. They called it CoReHA which stands for conductivity reconstructor using harmonic algorithms. It offers various computational tools including preprocessing of MREIT data, image segmentation for extraction of boundary geometry, electrode shape and positions, denoising [30], [31], harmonic inpainting [32], conductivity image reconstruction, postprocessing and visualization. Since CoReHA automated most parts of data processing tasks in MREIT, we utilized it to process the *in vivo* human experiment data and produce conductivity images.

III. Results

Fig. 2(a) is a typical MR magnitude image of the leg from the first subject (male A). Fig. 2(b) and (c) are measured B_z images in the same slice for horizontal and vertical current injections, respectively. In Fig. 2(a), we can see that MR signal void occurred in the outer layers of the bones. Since the noise level in measured B_z data is inversely proportional to the signal-to-noise ratio (SNR) of the MR magnitude image [33], [34], we can see that B_z images in Fig. 2(b) and (c) contains excessive amounts of noise in the outer layers of the bones.

Fig. 3 compares the anatomy of the leg in (a) [35] with an MR magnitude image in (b) and a reconstructed conductivity image in (c). The conductivity image exhibits spurious noise spikes in the outer layers of the bones due to a high noise level in B_z data there. Except those problematic regions, it well distinguishes the subcutaneous adipose tissue and different parts of the muscle. In the internal region of the bone corresponding to the yellow marrow, reconstructed conductivity values are lower than that of the muscle. We can clearly see that conductivity values of the crural fascia and intermuscular septum are relatively higher than that of the muscle.

In Figs. 4–7, we have shown multislice conductivity images of the four human subjects. For the three subjects shown in Figs. 4–6, we can observe the chemical shift of about two pixels around the subcutaneous adipose tissue. In Fig. 7, we have shown images of the fourth subject (female B) using the fat suppression method. Images in the first and second rows are MR magnitude images without and with using the fat suppression method, respectively. We can see that the fat suppression deteriorates the magnitude image SNR though it

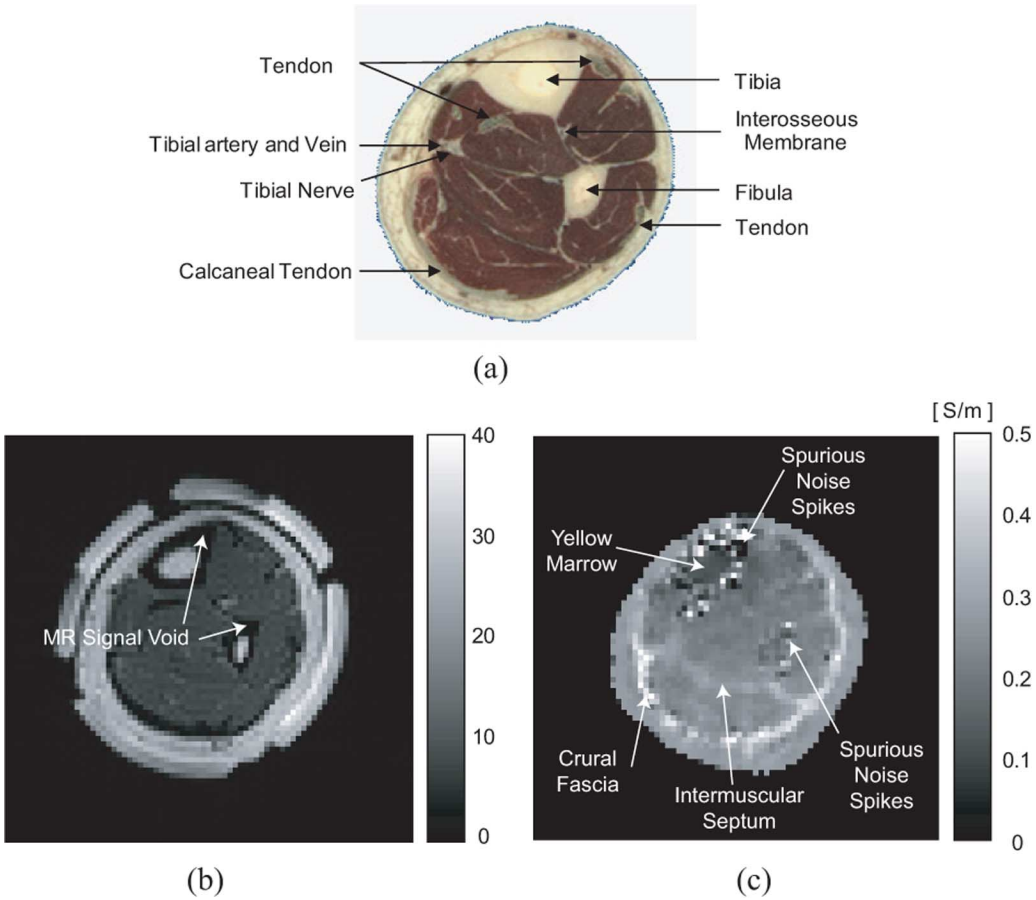

Fig. 3. (a) Typical anatomical structure of the human leg. (b) and (c) MR magnitude and reconstructed conductivity images, respectively, of the leg from the first subject (male A).

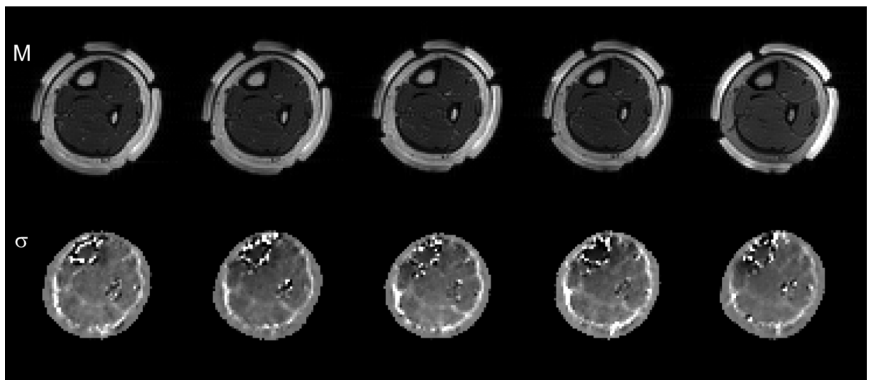

Fig. 4. Multislice MR magnitude (M) and reconstructed conductivity (σ) images of the leg from the first subject (male A).

relieves the chemical shift problem. The reduced SNR resulted in a higher noise level in measured B_z images. Consequently, the reconstructed conductivity images shown in the third row of Fig. 7 exhibit more noise.

IV. Discussion

In this paper, we have reported the first MREIT experiment of the human subject. Numerous previous MREIT experiments of postmortem and *in vivo* animals enabled us to design the human experiment and successfully produce *in vivo* conductivity images of the human leg with a pixel size of 1.7 mm. Use of flexible and large carbon–hydrogel electrodes allowed us to inject as much as 9 mA current in a form of 15 ms pulse with a tolerable amount of sensation and motion artifact. Reconstructed conductivity images show quite different and unique contrast information compared with conventional MR magnitude images. Though the adopted experimental protocol was successfully implemented in this first MREIT human imaging experiment, it seems to be too primitive to be used in clinical environments.

In this first human imaging experiment, we chose the lower extremity as the imaging region primarily due to the issue of electrical safety. The IEC 60601–1 defines the patient auxiliary current that is limited by 10 $\mu\mathrm{A}_{\mathrm{rms}}$ for frequencies below 1 kHz [37]. The IEC 60601-2-10 defines the therapeutic current and also the diagnostic current for dentistry and ophthalmology [38].

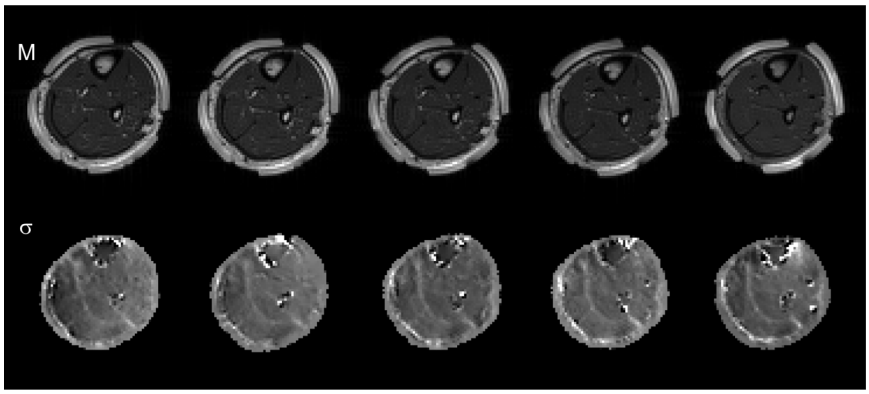

Fig. 5. Multislice MR magnitude (M) and reconstructed conductivity (σ) images of the leg from the second subject (male B).

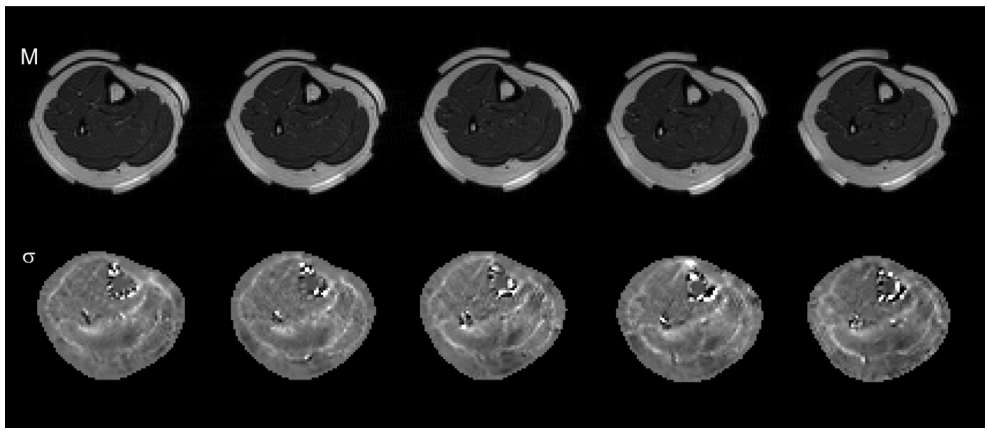

Fig. 6. Multislice MR magnitude (M) and reconstructed conductivity (σ) images of the leg from the third subject (female A).

Limits for these currents are significantly higher than the patient auxiliary current. For intermittent injections of current pulses used in MREIT, we speculate that the limit for the imaging current should be determined differently from the patient auxiliary current. Further investigation is requested regarding the electrical safety of the imaging current used in MREIT.

Since we produced scaled conductivity images using the single-step harmonic B_z algorithm [23], they provide only contrast information. This means that we should not view reconstructed conductivity values of different tissues as their absolute conductivity values. Comparing with previous experimental results summarized in [10], we may assume that the amount of noise in B_z data was not large enough to reverse the conductivity contrast. Based on this assumption, we examined reconstructed conductivity values of different tissues.

The crural fascia and intermuscular septum appear as more conductive regions compared with the muscle probably due to conductive fluids in those regions. Conductivity of the yellow marrow inside the bone is lower than that of the muscle. We could not correctly recover a conductivity value of the compact bone in this paper. Assuming that the compact bone has a quite small conductivity value, injection currents at two different directions may have produced almost parallel current densities around its boundary. When this happens, the harmonic B_z algorithm fails to recover a correct conductivity value around the boundary [36]. In addition, the MR signal void phenomenon occurred in the compact bone causing a large noise level there in measured B_z data. In order to alleviate these technical problems, a more sophisticated implementation of the local harmonic B_z algorithm will be necessary in future work [23].

Previous studies reported that the muscle conductivity along its transversal direction is higher than the conductivity of the fat [24]–[27]. Our results indicate that the subcutaneous adipose tissue has a similar conductivity value compared with that of the muscle. We speculate that body fluids surrounding the adipose tissue increase its conductivity value in *in vivo* measurements. This may exhibit the importance of the *in vivo* conductivity measurement of a tissue in a living wetted state by using the MREIT technique. We, however, would like to defer ascertaining the statement about the conductivity of the *in vivo* subcutaneous adipose tissue since our results could have been affected by the chemical shift effects of the fat.

Individual variations in morphology, size, and tissue composition affect the quality and contrast of reconstructed conductivity images. Imaging parameters such as the current amplitude, current pulse width and details of MR pulse sequence also significantly affect the image quality. As shown in Table I, we used 7 mA injection currents for the second subject (male B) while we injected 9 mA into other three subjects. This should have caused the conductivity images of the second subject in Fig. 5 to have an increased noise level.

The conductivity images from the fourth subject (female B) in Fig. 7 are more noisier due to a different reason. Unlike the postmortem and *in vivo* canine brain imaging experiments [15],

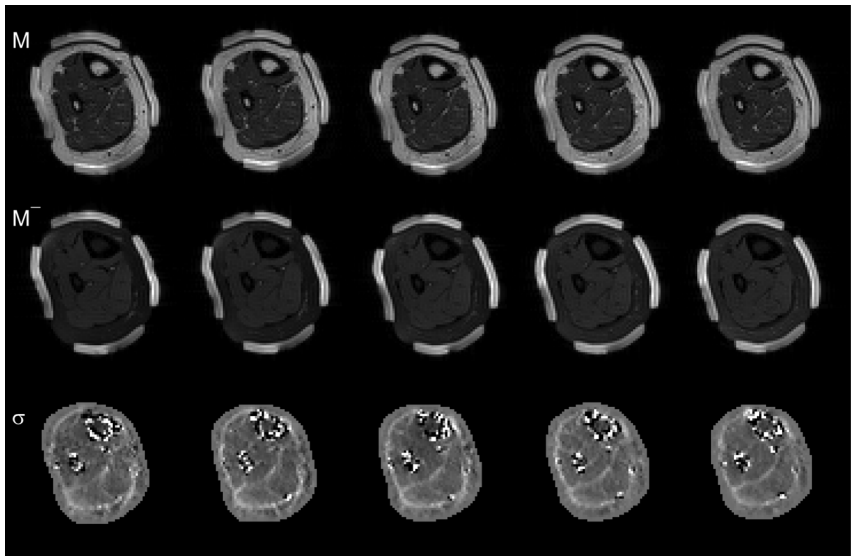

Fig. 7. Images of the leg from the fourth subject (female B). The first and second rows show multislice MR magnitude images without (M) and with (M^-) using a fat suppression, respectively. Reconstructed conductivity images (σ) are in the third row.

[16], the *in vivo* human leg imaging experiments revealed the problem of the chemical shift in the fat region. We have tested a fat suppression method for the fourth subject but it significantly reduced the magnitude image SNR and increased the noise level in conductivity images as shown in Fig. 7. Instead, we could have decreased the dwell time to make the chemical shift occur within one pixel but this would also reduce the SNR. Since the noise level in a measured B_z image is inversely proportional to the magnitude image SNR [33], [34], these methods are not desirable in MREIT. This means that, in our future work, we have to incorporate a fat correction method in the MREIT pulse sequence.

The conductivity images of the normal leg themselves do not convey much information with clinical significance other than those discussed above. There are numerous potential clinical applications of MREIT as discussed in [10]. In order to find its feasibility as a new medical imaging modality with clinical significance, we need to apply it to other parts of the human body. In future studies, we plan to perform MREIT imaging experiments of the abdomen, pelvis, head, and chest. The most critical requirement is the reduction of the injection current to a safe level. The safe level does not mean a level where no physiological effect occurs. It should mean a level where the internal current density does not produce an irreversible undesirable effect.

In this paper, we used the harmonic B_z algorithm since it is implemented in CoReHA [29] and we are most familiar with it. There are several other MREIT image reconstruction algorithms [39]–[46]. It would be desirable to compare performances of those algorithms using the same data sets from phantom, animal and human experiments. Choosing the best algorithm or designing a hybrid algorithm, there is a room to improve the image quality in future work.

V. Conclusion

In MREIT, we are facing a few technical difficulties to reach the stage of clinical applications. First, we must improve the conductivity image reconstruction algorithm so that we can effectively handle the MR signal void phenomenon. Second, effects of tissue anisotropy should be understood in relation with the data collection method and image reconstruction algorithm. These algorithmic improvements should provide a more solid basis for unambiguous interpretation of a reconstructed scaled equivalent isotropic conductivity image.

Third, we should investigate how much imaging current can be safely injected into the human subject. We should note that the current is intermittently injected in a form of a short pulse. We should focus on the distribution of the current density underneath the electrode and inside the human body instead of the total current. Factors such as the electrode design including its shape, size, and material as well as positions of electrodes and choice of imaging area should be considered. We may consider building a safety standard for the imaging current as proposed in [10]. Fourth, MR imaging techniques and parameters like the RF coil and pulse sequence must be optimized to reduce the total imaging time. We may significantly improve the SNR by using phase array coils. Fifth, numerous pre- and post-processing techniques need to be developed for better image quality.

Focusing our research efforts on finding solutions to the above mentioned technical problems, we plan to perform numerous *in vivo* animal and human experiments to advance the MREIT technique to the stage of clinical uses. In doing so, we should take account of possible application areas discussed in [16] and [10].

References

[1] D. Holder, *Electrical Impedance Tomography: Methods, History and Applications*. Bristol, U.K.: IOP Publishing, 2005.

[2] B. I. Lee, S. H. Oh, E. J. Woo, S. Y. Lee, M. H. Cho, O. Kwon, J. K. Seo, J. Y. Lee, and W. S. Baek, "Three-dimensional forward solver and its performance analysis in magnetic resonance electrical impedance tomography (MREIT) using recessed electrodes," *Phys. Med. Biol.*, vol. 48, pp. 1971–1986, 2003.

[3] G. C. Scott, M. L. G. Joy, R. L. Armstrong, and R. M. Henkelman, "Measurement of nonuniform current density by magnetic resonance," *IEEE Trans. Med. Imag.*, vol. 10, pp. 362–374, Oct. 1991.

[4] N. Zhang, "Electrical impedance tomography based on current density imaging," M.S. degree, Dept. Elec. Eng., Univ. Toronto, Toronto, ON, Canada, 1992.

[5] E. J. Woo, S. Y. Lee, and C. W. Mun, "Impedance tomography using internal current density distribution measured by nuclear magnetic resonance," *Proc. SPIE*, vol. 2299, pp. 377–385, 1994.

[6] O. Birgul and Y. Z. Ider, "Use of the magnetic field generated by the internal distribution of injected currents for electrical impedance tomography," in *Proc. IXth Int. Conf. Elec. Bio-Impedance*, Heidelberg, Germany, 1995, pp. 418–419.

[7] Y. Z. Ider and O. Birgul, "Use of the magnetic field generated by the internal distribution of injected currents for electrical impedance Tomography(MR-EIT)," *Elektrik*, vol. 6, no. 3, pp. 215–225, 1998.

[8] O. Kwon, E. J. Woo, J. R. Yoon, and J. K. Seo, "Magnetic resonance electrical impedance tomography (MREIT): Simulation study of J-substitution algorithm," *IEEE Trans. Biomed. Eng.*, vol. 49, no. 2, pp. 160–167, Feb. 2002.

[9] E. J. Woo, J. K. Seo, and S. Y. Lee, "Magnetic resonance electrical impedance tomography (MREIT)," in *Electrical Impedance Tomography: Methods, History and Applications*, D. Holder, Ed. Bristol, U.K.: IOP Publishing, 2005.

[10] E. J. Woo and J. K. Seo, "Magnetic resonance electrical impedance tomography (MREIT) for high-resolution conductivity imaging," *Physiol. Meas.*, vol. 29, pp. R1–R26, 2008.

[11] S. H. Oh, B. I. Lee, E. J. Woo, S. Y. Lee, M. H. Cho, O. Kwon, and J. K. Seo, "Conductivity and current density image reconstruction using harmonic B_z algorithm in magnetic resonance electrical impedance tomography," *Phys. Med. Biol.*, vol. 48, pp. 3101–3016, 2003.

[12] S. H. Oh, B. I. Lee, T. S. Park, S. Y. Lee, E. J. Woo, M. H. Cho, O. Kwon, and J. K. Seo, "Magnetic resonance electrical impedance tomography at 3 tesla field strength," *Mag. Reson. Med.*, vol. 51, pp. 1292–1296, 2004.

[13] S. H. Oh, B. I. Lee, E. J. Woo, S. Y. Lee, T. S. Kim, O. Kwon, and J. K. Seo, "Electrical conductivity images of biological tissue phantoms in MREIT," *Physiol. Meas.*, vol. 26, pp. S279–S288, 2005.

[14] L. T. Muftuler, M. J. Hamamura, O. Birgul, and O. Nalcioglu, "In vivo MRI electrical impedance tomography (MREIT) of tumors," *Technol. Cancer Res. Treat.*, vol. 5, pp. 381–387, 2006.

[15] H. J. Kim, B. I. Lee, Y. Cho, Y. T. Kim, B. T. Kang, H. M. Park, S. L. Lee, J. K. Seo, and E. J. Woo, "Conductivity imaging of canine brain using a 3 T MREIT system: Postmortem experiments," *Physiol. Meas.*, vol. 28, pp. 1341–1353, 2007.

[16] H. J. Kim, T. I. Oh, Y. T. Kim, B. I. Lee, E. J. Woo, J. K. Seo, S. Y. Lee, O. Kwon, C. Park, B. T. Kang, and H. M. Park, "In vivo electrical conductivity imaging of a canine brain using a 3 T MREIT system," *Physiol. Meas.*, vol. 29, pp. 1145–1155, 2008.

[17] E. J. Woo, H. J. Kim, A. S. Minhas, Y. T. Kim, W. C. Jeong, and O. J. Kwon, "Electrical conductivity imaging of lower extremities using MREIT: Postmortem swine and in vivo human experiments," in *Proc. 30th Ann. Int. IEEE EMBS Conf.*, Vancouver, BC, Canada, 2008, pp. 5830–5833.

[18] A. S. Minhas, W. C. Jeong, Y. T. Kim, H. J. Kim, T. H. Lee, and E. J. Woo, "MREIT of postmortem swine legs using carbon-hydrogel electrodes," *J. Biomed. Eng. Res.*, vol. 29, pp. 436–442, 2008.

[19] T. I. Oh, Y. Cho, Y. K. Hwang, S. H. Oh, E. J. Woo, and S. Y. Lee, "Improved current source design to measure induced magnetic flux density distributions in MREIT," *J. Biomed. Eng. Res.*, vol. 27, pp. 30–37, 2006.

[20] C. Park, B. I. Lee, O. Kwon, and E. J. Woo, "Measurement of induced magnetic flux density using injection current nonlinear encoding (ICNE) in MREIT," *Physiol. Meas.*, vol. 28, pp. 117–127, 2006.

[21] J. Mao, H. Han, and W. D. Bidgood, "Fat suppression with an improved selective presaturation pulse," *Mag. Reson. Imag.*, vol. 10, no. 1, pp. 49–53, 1992.

[22] J. K. Seo, J. R. Yoon, E. J. Woo, and O. Kwon, "Reconstruction of conductivity and current density images using only one component of magnetic field measurements," *IEEE Trans. Biomed. Eng.*, vol. 50, no. 9, pp. 1121–1124, Sep. 2003.

[23] J. K. Seo, S. W. Kim, S. Kim, J. Liu, E. J. Woo, K. Jeon, and C. O. Lee, "Local harmonic B_z algorithm with domain decomposition in MREIT: Computer simulation study," *IEEE Trans. Med. Imag.*, vol. 27, no. 12, pp. 1754–1761, Dec. 2008.

[24] C. Gabriel, S. Gabriel, and E. Corthout, "The dielectric properties of biological tissues: I. Literature survey," *Phys. Med. Biol.*, vol. 41, pp. 2231–2249, 1996.

[25] S. Gabriel, R. W. Lau, and C. Gabriel, "The dielectric properties of biological tissues: II. Measurements in the frequency range 10Hz to 20GHz," *Phys. Med. Biol.*, vol. 41, pp. 2251–2269, 1996.

[26] L. A. Geddes and L. E. Baker, "The specific resistance of biological material: A compendium of data for the biomedical engineer and physiologist," *Med. Biol. Eng.*, vol. 5, pp. 271–293, 1967.

[27] S. Grimnes and O. G. Martinsen, *Bioimpedance and Bioelectricity Basics*, 2nd ed. Oxford, U.K.: Academic, 2008.

[28] T. S. Kim, B. I. Lee, C. Park, S. H. Lee, S. H. Tak, J. K. Seo, O. Kwon, and E. J. Woo, "A Matlab toolbox for magnetic resonance electrical impedance tomography (MREIT): MREIT toolbox," *IJBEM*, vol. 7, pp. 352–355, 2005.

[29] K. Jeon, C. O. Lee, E. J. Woo, and J. K. Seo, "Coreha: Conductivity reconstructor using harmonic algorithms for magnetic resonance electrical impedance tomography (MREIT)," *Comp. Meth. Prog. Biomed.*, 2008, submitted for publication.

[30] B. I. Lee, S. H. Lee, T. S. Kim, O. Kwon, E. J. Woo, and J. K. Seo, "Harmonic decomposition in PDE-based denoising technique for magnetic resonance electrical impedance tomography," *IEEE Trans. Biomed. Eng.*, vol. 52, no. 11, pp. 1912–1920, Nov. 2005.

[31] B. I. Lee, C. Park, H. C. Pyo, O. Kwon, and E. J. Woo, "Phase artifact reduction in magnetic resonance electrical impedance tomography (MREIT)," *Phys. Med. Biol.*, vol. 51, pp. 5277–5288, 2006.

[32] S. Lee, J. K. Seo, C. Park, B. I. Lee, E. J. Woo, S. Y. Lee, O. Kwon, and J. Hahn, "Conductivity image reconstruction from defective data in MREIT: Numerical simulation and animal experiment," *IEEE Trans. Med. Imag.*, vol. 25, no. 2, pp. 168–176, Feb. 2006.

[33] G. C. Scott, M. L. G. Joy, R. L. Armstrong, and R. M. Henkelman, "Sensitivity of magnetic-resonance current density imaging," *J. Mag. Res.*, vol. 97, pp. 235–254, 1992.

[34] R. Sadleir, S. Grant, S. U. Zhang, B. I. Lee, H. C. Pyo, S. H. Oh, C. Park, E. J. Woo, S. Y. Lee, O. Kwon, and J. K. Seo, "Noise analysis in magnetic resonance electrical impedance tomography at 3 and 11 T field strengths," *Physiol. Meas.*, vol. 26, pp. 875–884, 2005.

[35] The internet pathology laboratory for medical education Univ. Utah, Salt Lake City, 2009 [Online]. Available: http://library.med.utah.edu/WebPath/

[36] J. J. Liu, J. K. Seo, M. Sini, and E. J. Woo, "On the convergence of the harmonic B_z algorithm in magnetic resonance electrical impedance tomography," *SIAM J. Appl. Math.*, vol. 67, no. 5, pp. 1259–1282, 2007.

[37] Medical electrical equipment—Part1: General requirements for basic safety and essential performance IEC, Geneva, Switzerland, 2005.

[38] Medical electrical equipment—Part2–10: Particular requirements for the safety of nerve and muscle stimulators IEC, Geneva, Switzerland, 2001.

[39] Y. Z. Ider and O. Birgul, "Use of the magnetic field generated by the internal distribution of injected currents for electrical impedance tomography," *Elektrik*, vol. 6, pp. 215–225, 1998.

[40] S. Onart, Y. Z. Ider, and W. Lionheart, "Uniqueness and reconstruction in magnetic resonance-electrical impedance tomography (MR-EIT)," *Physiol. Meas.*, vol. 24, pp. 591–604, 2003.

[41] C. Park, O. Kwon, E. J. Woo, and J. K. Seo, "Electrical conductivity imaging using gradient B_z decomposition algorithm in magnetic resonance electrical impedance tomography (MREIT)," *IEEE Trans. Med. Imag.*, vol. 23, no. 3, pp. 388–394, Mar. 2004.

[42] C. Park, E. J. Park, E. J. Woo, O. Kwon, and J. K. Seo, "Static conductivity imaging using variational gradient B_z algorithm in magnetic resonance electrical impedance tomography," *Physiol. Meas.*, vol. 25, pp. 275–269, 2004.

[43] N. Gao, S. A. Zhu, and B. He, "New magnetic resonance electrical impedance tomography (MREIT) algorithm: The RSM-MREIT algorithm with applications to estimation of human head conductivity," *Phys. Med. Biol.*, vol. 51, pp. 3067–3083, 2006.

[44] C. Park, B. I. Lee, and O. Kwon, "Analysis of recoverable current from one component of magnetic flux density in MREIT and MRCDI," *Phys. Med. Biol.*, vol. 52, pp. 3001–3013, 2007.

[45] H. S. Nam, B. I. Lee, J. Choi, C. Park, and O. Kwon, "Conductivity imaging with low level of current injection using transversal J-substitution algorithm in MREIT," *Phys. Med. Biol.*, vol. 52, pp. 6717–6730, 2007.

[46] N. Gao and B. He, "Noninavsive imaging of bioimpedance distribution by means of current reconstruction magnetic resonance electrical impedance tomography," *IEEE Trans. Biomed. Eng.*, vol. 55, pp. 1530–1538, 2008.